HOKKAIDO UNIVERSITY

Title	Intravoxel incoherent motion diffusion-weighted imaging in head and neck squamous cell carcinoma : Assessment of perfusion-related parameters compared to dynamic contrast-enhanced MRI
Author(s)	Fujima, Noriyuki; Yoshida, Daisuke; Sakashita, Tomohiro et al.
Citation	Magnetic resonance imaging, 32(10), 1206-1213 https://doi.org/10.1016/j.mri.2014.08.009
Issue Date	2014-12
Doc URL	https://hdl.handle.net/2115/57770
Type	journal article
File Information	manuscript1.pdf

Hokkaido University Collection of Scholarly and Academic Papers : HUSCAP

ORIGINAL ARTICLE

Intravoxel Incoherent Motion Diffusion-Weighted Imaging in Head and Neck Squamous Cell Carcinoma: Assessment of Perfusion-Related Parameters Compared to Dynamic Contrast-Enhanced MRI

Noriyuki Fujima, MD, PhD[1,*]; Daisuke Yoshida, MD[1]; Tomohiro Sakashita, MD, PhD[2]; Akihiro Homma, MD, PhD[2]; Akiko Tsukahara, MD[1]; Khin Khin Tha, MD, PhD[3]; Kohsuke Kudo, MD, PhD[1]; and Hiroki Shirato, MD, PhD[3]

[1]Department of Diagnostic and Interventional Radiology, Hokkaido University Hospital, Sapporo, Japan

Departments of [2]Otolaryngology-Head and Neck Surgery and [3]Radiation Medicine, Hokkaido University Graduate School of Medicine, Sapporo, Japan

ABSTRACT

Purpose: To investigate the correlation between perfusion-related parameters obtained with intravoxel incoherent motion (IVIM) and classical perfusion parameters obtained with dynamic contrast-enhanced (DCE) MRI in patients with head and neck squamous cell carcinoma (HNSCC), and to compare direct and asymptotic fitting, the pixel-by-pixel approach, and a region of interest (ROI)-based approach respectively for IVIM parameter calculation.

Materials and Methods: Seventeen patients with HNSCC were included in this retrospective study. All MR scanning was performed using a 3T MR unit. Acquisition of IVIM was performed using single-shot spin-echo echo-planar imaging with three orthogonal gradients with 12 b-values (0, 10, 20, 30, 50, 80, 100, 200, 400, 800, 1000, and 2000). Perfusion-related parameters of perfusion fraction 'f' and the pseudo-diffusion coefficient 'D*' were calculated from IVIM data by using least square fitting with the two fitting methods of direct and asymptotic fitting, respectively. DCE perfusion was performed in a total of 64 dynamic phases with a 3.2-s phase interval. The two-compartment exchange model was used for the quantification of tumor blood volume (TBV) and tumor blood flow (TBF). Each tumor was delineated with a polygonal ROI for the calculation of f, f·D* performed using both the pixel-by-pixel

approach and the ROI-based approach. In the pixel-by-pixel approach, after fitting each pixel to obtain f, f·D* maps, the mean value in the delineated ROI on these maps was calculated. In the ROI-based approach, the mean value of signal intensity was calculated within the ROI for each b-value in IVIM images, and then fitting was performed using these values. Correlations between f in a total of four combinations (direct or asymptotic fitting and pixel-by-pixel or ROI-based approach) and TBV were respectively analyzed using Pearson's correlation coefficients. Correlations between f·D* and TBF were also similarly analyzed.

Results: In all combinations of f and TBV, f·D* and TBF, there was a significant correlation. In the comparison of f and TBV, a moderate correlation was observed only between f obtained by direct fitting with the pixel-by-pixel approach, whereas a good correlation was observed in the comparisons using the other three combinations. In the comparison of f·D* and TBF, a good correlation was observed only with f·D* obtained by asymptotic fitting with the ROI-based approach. In contrast, moderate correlations were observed in the comparisons using the other three combinations.

Conclusion: IVIM was found to be feasible for the analysis of perfusion-related parameters in patients with HNSCC. Especially, the combination of asymptotic fitting with the ROI-based approach was better correlated with DCE perfusion.

INTRODUCTION

Tumor diffusion and perfusion are important biological parameters for the assessment of head and neck squamous cell carcinoma (HNSCC), and their usefulness has been described for the first assessments for treatment planning, the early detection of treatment effect, and post-treatment assessments to detect the presence of residual tumor [1]. Estimations of tumor perfusion have been performed mainly by the dynamic contrast-enhanced (DCE) technique [2, 3]. This technique has been used widely for the assessment of tumor perfusion in HNSCC [4-7].

Intravoxel incoherent motion (IVIM) imaging was introduced to assess both tumor diffusion and perfusion noninvasively by analyzing the signal decay curve obtained from multiple b-value diffusion-weighted imaging (DWI) acquisition to separate the signal intensity arising from a vascular component and that from a nonvascular component [8]. In IVIM imaging, two perfusion-related parameters, the perfusion fraction “f” and the pseudo-diffusion coefficient “D*” and one diffusion-related parameter of the slow diffusion coefficient “D” are calculated. The symbol “D*” represents the fast diffusion which is related to the microvascular compartment under the assumption that the microvascular network is isotropic and sufficiently random so that the movement of the water in blood is incoherent. In contrast, the letter “D”

represents the water diffusion of the nonvascular compartment estimated approximately tens of micrometers [9], and is smaller than D*. The letter “f” represents the percentage of incoherent signal which is assumed to arise mainly from the fast diffusion of microvascular compartment. These three parameters can be calculated by fitting the diffusion-weighted signal intensity of multiple b-value images to a bi-exponential model as described [10]. However, the perfusion-related parameters f and D* were reported to tend to be unstable in IVIM fitting and to sometimes result in incorrect values [11, 12].

Several comparative studies were performed to investigate the correlation of perfusion estimation by IVIM in, for example, normal brain tissue, brain tumor, and prostate cancer [12-14]. Although a few investigations of the clinical utility of IVIM imaging in patients with HNSCC were performed [9, 15], no study has assessed the correlation of IVIM parameters in HNSCC by comparing IVIM imaging results to other modalities, such as MR perfusion (DCE perfusion and dynamic susceptibility contrast perfusion) or CT perfusion. Head and neck lesions in particular can be influenced by the susceptibility effect, which results in incorrect signal intensity or image distortion [16]. A study of perfusion estimation by IVIM imaging compared to that achieved with other methods for patients with HNSCC is thus necessary.

The aim of the present study was to determine the correlation between

perfusion-related parameters obtained with IVIM imaging with various calculation methods and perfusion parameters obtained with the dynamic contrast-enhanced (DCE) perfusion technique.

MATERIALS AND METHODS

Subjects

The study protocol was approved by our institutional review board. Seventeen patients were evaluated retrospectively with the following inclusion criteria: (1) the patient was diagnosed histopathologically as having HNSCC, (2) MR scanning was performed before any treatment, and (3) MR scans with both IVIM and DCE perfusion were performed within the same examination. The patients were 15 males (mean age 62 years; range 45–79 years) and two females (49 and 53 years old). The primary sites of the 17 patients were the maxillary sinus in six patients, the tongue in six patients, and the oropharynx in five patients.

MR imaging protocol

All MR imaging was performed using a 3.0 Tesla unit (AchievaTX; Philips Medical Systems, Best, the Netherlands) with a 16-channel neurovascular coil.

Acquisition of IVIM was performed by using single-shot spin-echo echo-planar imaging (EPI) with three orthogonal motion probing gradients. Twelve b-values (0, 10, 20, 30, 50, 80, 100, 200, 400, 800, 1000, and 2000) were used. The other MR parameters were as follows: TR, 4500 ms; TE, 64 ms; DELTA (large delta), 30.1 ms; delta (small delta), 24.3 ms; flip angle, 90°; FOV, 230 × 230 mm; 64 × 64 matrix; slice thickness, 5 mm × 20 slices; parallel imaging acceleration factor, 2; scanning time, 4 min 37 s. Patients were instructed not to swallow, move their tongues, open their mouths, or make any other voluntary motion before the IVIM scanning. In addition, their heads were fixed firmly with the coil to prevent movement during scanning.

The DCE perfusion data were acquired after a bolus injection of 0.2 mmol gadolinium/kg (gadopentetate dimuglumine; Magnevist, Bayern Schering Pharma AG, or gadodiamide; Omniscan, GE healthcare) using a power injector at a rate of 2 mL/s, followed by 15 mL of saline flush. Image acquisition was performed using a three-dimensional (3D)-T1 fast field echo (T1-FFE) sequence. This sequence also contained the pre-scan to obtain the T1 map as a reference before a bolus injection. The MR parameters for dynamic data acquisition were as follows: TR, 6.1 ms; TE, 1.5 ms; flip angle, 15°; temporal resolution, 3.2 s; dynamic phase, 64 phases; matrix, 256 × 256 in 230 × 230 mm FOV (pixel size, 0.94 × 0.93 mm); slice thickness, 3 mm × 31 slices;

scanning time, 3 min 51 s.

After the acquisition of the DCE perfusion sequence, post-contrast-enhanced 3D-T1WI was also obtained for the reference of tumor delineation to determine the tumor region of interest (ROI). This sequence was performed using a 3D spoiled gradient echo sequence with the following parameters: TR, 3.7 ms; TE, 1.6 ms; TFE factor, 48; flip angle, 15°; FOV, 230 × 230 mm; 512 × 512 matrix; slice thickness, 1.0 mm × 350 slices; scanning time, 3 min 51 s.

Analysis of IVIM data

We calculated the IVIM parameters (fraction f, pseudo-diffusion coefficient D*, and slow diffusion coefficient D) from the signal intensity of multiple b-values in the IVIM data. To obtain these IVIM parameters, we applied the image signal intensity of each b-value to the following bi-exponential function [8]:

$$\frac{S_{(b)}}{S_0} = f \cdot e^{-b \cdot D^*} + (1 - f) \cdot e^{-b \cdot D} \quad (1)$$

where $S_{(b)}$ is the signal intensity at the b-value denoted by the subscript, and S_0 is the signal intensity at the b-value of 0. We fitted the signal intensity of each b-value in Eq.

[1] with least square fitting using the Levenberg-Marquardt algorithm. Two fitting methods were used for the calculation: (1) direct fitting, in which the three parameters were respectively calculated by using direct fitting to Eq. (1) using the image signal intensity in each b-value, and (2) asymptotic fitting, to increase the robustness of the fitting with less calculation error. The following two steps for asymptotic fitting were performed. First, the data of b>200 s/mm^2 were fitted for the single parameter D, because D* is assumed to be significantly greater than D, so that the influence of pseudo-diffusion on signal decay can be neglected for b-values greater than 200 s/mm^2 [10]. In the second step, the curve was fitted for f and D* over all b-values, while keeping D constant. In each method, to convert general perfusion parameters such as blood volume and blood flow, because the theoretical relationships between (1) the IVIM perfusion parameter f and the classical perfusion parameter TBV (tumor blood volume), and (2) the IVIM parameter f·D* (the multiplication of the two parameters) and the classical perfusion parameter TBF (tumor blood flow) were described with following equations: $f = \lambda_{H2O}^{\wedge}(-1) \cdot TBV$, $f \cdot D^* = [L \cdot \langle l \rangle / 6 \lambda_{H2O}^{\wedge}(-1)] \cdot TBF$ (λ_{H2O}: the fraction of MRI visible water, L: the distance between the entry and the exit of the microvascular network, <l>: the mean microvessel length), combinations of these parameters were used respectively for the comparison to DCE perfusion [13].

Analysis of DCE perfusion data

TBV and TBF calculations using DCE perfusion were conducted according to the method described based on the two-compartment model (Fig. 1) [17]. Tissue blood flow can be obtained with the following equation from the assumption that tumor tissue concentration changes in dynamic data can be obtained from the difference between the concentration of the arterial inlet and the outflow of plasma:

$$\frac{dC}{dt}(t) = F \cdot (1 - Hct) \cdot \left(C_a(t) - C_p(t)\right) \quad (2)$$

where C(t) (mmol/mL) is the contrast agent concentration in tissue, F is the tissue blood flow (mL/100g/min), $C_a(t)$ (mmol/mL) is the incoming plasma concentration of the contrast agent from the arterial inlet, $C_p(t)$ (mmol/mL) is the outgoing plasma concentration of the contrast agent, and Hct is the hematocrit of a small artery assumed to be 0.33 [17]. We measured $C_a(t)$ from the signal intensity in the region of arterial blood near the primary tumor.

To measure $C_p(t)$, in addition, by using a two-compartment model of tissue plasma and extravascular extracellular space (EES), the plasma concentration change was

assumed from a mass balance for a capillary compartment of the arterial inlet, the outflow of plasma, and the permeability surface product with following equation:

$$v_p \frac{dC_p}{dt} = F \cdot C_a(t) - C_p(t) \cdot (F + PS) \tag{3}$$

where PS is the permeability-surface product (min^{-1}), and v_p is the plasma volume fraction. The signal intensity was converted into concentration equivalents assuming a near-linear relationship between the contrast media and the signal increase defined by the following equation [18, 19]:

$$(S(t) - S(0)) / S(0) \propto C(t) \tag{4}$$

The time course of the dynamic data was fitted to Eqs. [2] and [3] for the calculation of F and v_p. Finally, the following equations were used for the calculation of TBV and TBF [17]:

$$\begin{aligned} F &= TBF \\ v_p &= TBV \cdot (1 - Hct) \end{aligned} \tag{5}$$

where Hct is the hematocrit of a small artery assumed to be 0.33 the same as Eq. [2] [20]. In the case of v_p, the TBV calculation was performed with the modification of the percentage of red blood cells by using the value of the hematocrit. Finally, respective TBV and TBF maps were obtained on a pixel-by-pixel basis.

All calculations of signal intensity were performed using mathematical software (MATLAB, version 2012a) in both the IVIM and DCE perfusion analyses.

ROI delineation and parameter calculations

Each tumor was delineated with a polygonal ROI on b0 images in the IVIM analysis, and with the latest phase of the DCE raw data in the DCE perfusion analysis by a board-certified neuroradiologist with 17 years of experience. Post-contrast-enhanced 3D-T1WI images were used as reference images for the delineation. If the tumor extended into two or more slices, all slices in which the tumor was included were used for the ROI delineation. The IVIM parameter calculation was performed by (1) the pixel-by-pixel approach and (2) the ROI-based approach. In the pixel-by-pixel approach, an f map and an f・D* map were each obtained on a pixel-by-pixel basis from each pixel's signal intensity in IVIM data using both direct

and asymptotic fitting respectively.Each delineated tumor ROI was copied on the f and f·D* maps in the IVIM analysis (Fig. 2). Each f-value and f·D* value in the IVIM analysis was determined as the mean value in the delineated ROI by integrating all tumor voxels from all delineated slices into the total signal intensity. For each pixel, the upper and lower limits were set for each calculated value to exclude unrealistic measurement (probably because of several outliers) to avoid including any erroneous pixels in the calculation. The lower and upper limits of f and D* were respectively set at 0 – 0.4, and 0 – 50×10^{-3} by referring the range of each parameters in to an earlier report [9]. In the ROI-based approach, the IVIM parameter calculations were performed as follows: (1) each tumor ROI was copied in EPI images of IVIM for each b-value, (2) the mean value of these ROIs were defined as the image signal intensity for each b-value, and (3) by using the mean signal intensity in the ROI for each b-value, the IVIM parameters of f and f・D* were calculated using both direct and asymptotic fitting (Fig. 3).

The calculations of TBV and TBF were performed by the same method used for the IVIM parameter calculation in the pixel-by-pixel approach as follows: the delineated tumor ROI in DCE raw image was copied on the respective TBV and TBF maps in the DCE analysis. Each TBV and TBF value was determined as the mean value in the

delineated ROI by integrating all tumor voxels from all delineated slices into the total signal intensity.

Statistical analysis

We analyzed the correlations between the f-values obtained with IVIM and the TBV values obtained with DCE perfusion using Pearson's correlation coefficients ($r < 0.2$, poor correlation; $r = 0.2–0.4$, fair correlation; $r = 0.41–0.6$, moderate correlation; $r = 0.61–0.8$, good correlation; $r \geq 0.81$, excellent correlation). We also analyzed the correlations between the f·D* values obtained with IVIM and the TBF values obtained with DCE perfusion. In both the IVIM perfusion-related parameters of f and f·D*, we analyzed four types of data by combinations of (1) direct or asymptotic fitting, and (2) the pixel-by-pixel approach or ROI-based approach. The following four combinations were respectively compared to the DCE perfusion parameter described above: (1) direct fitting with the pixel-by-pixel basis approach, (2) direct fitting with the ROI-based approach, (3) asymptotic fitting with the pixel-by-pixel approach, and (4) asymptotic fitting with the ROI-based approach. The level of significance was set at $p<0.05$.

RESULTS

MR scanning and image analyses of both IVIM and DCE perfusion were successfully performed in all 17 patients. The average of parameter f obtained with IVIM by the combination of direct fitting and the pixel-by-pixel approach was 0.20 ± 0.080; that with direct fitting with the ROI-based approach was 0.18 ± 0.043, that with asymptotic fitting with the pixel-by-pixel approach was 0.18 ± 0.045, and the value obtained with asymptotic fitting with the ROI-based approach was 0.17 ± 0.037. The average of TBV obtained with DCE perfusion was 14.2 ± 3.7 mL/100 mL.

All of the f values obtained with IVIM by these four types of methods had a significant correlation with TBV obtained with DCE perfusion (Fig. 4). In the combination of direct fitting with the pixel-by-pixel approach, a moderate correlation was observed between f and TBV ($r = 0.53$, $y = 0.011x - 0.046$, $p<0.05$). Compared to this result, the combination of asymptotic fitting with the pixel-by-pixel approach had a good correlation ($r = 0.65$, $y = 0.007x - 0.070$, $p<0.05$) (Fig. 5). In contrast, the ROI-based approach had a good correlation in both direct and asymptotic fitting (direct fitting; $r = 0.62$, $y = 0.007x - 0.073$, $p<0.05$, asymptotic fitting; $r = 0.68$, $y = 0.006x - 0.068$, $p<0.05$). The average of the parameter f・D* obtained with IVIM by the combination of direct fitting and the pixel-by-pixel approach was 3.3 ± 1.8 mm^2/s; that with direct fitting and the ROI-based approach was 2.6 ± 1.1 mm^2 /s, that with

asymptotic fitting and the pixel-by-pixel approach was 2.5 ± 1.4 mm^2 /s, and the average obtained with asymptotic fitting and the ROI-based approach was 2.2 ± 0.92 mm^2/s. The average of TBF obtained with DCE perfusion was 145.4 ± 28 mL/100g/min.

Each of the f·D* values obtained with IVIM by these four combinations also had a significant correlation with TBF obtained with DCE perfusion (Fig. 6). With only the combination of asymptotic fitting and the ROI-based approach, a good correlation between f·D* and TBF was observed ($r = 0.65$, $y = 0.021x - 0.92$, $p<0.05$). The correlation between f·D* obtained by each of the other three combinations and TBF was moderate (direct fitting with the pixel-by-pixel approach; $r = 0.47$, $y = 0.030x - 1.2$, $p<0.05$, asymptotic fitting with the pixel-by-pixel approach; $r = 0.54$, $y = 0.026x - 1.3$, $p<0.05$, direct fitting with the ROI-based approach; $r = 0.52$, $y = 0.019x - 0.27$, $p<0.05$).

DISCUSSION

The clinical usefulness of IVIM has been investigated in several organs in the body including liver, kidney, brain, and more [13, 21, 22]. Several investigations of the clinical utility of IVIM in patients with HNSCC were also reported [9, 15, 23]. However,

thorough comparisons of perfusion-related parameters obtained using IVIM with other modalities has not been conducted, although a few relevant studies were described for brain tissue, brain tumor, and prostate cancer; these studies assessed IVIM parameters by comparing a dynamic contrast perfusion technique or histopathological findings [13, 14, 24]. In particular, there has been no report comparing the perfusion-related parameters of IVIM to other modalities for the confirmation of its correlation in patients with HNSCC. In the present study, IVIM scanning in patients with HNSCC and the calculation of perfusion-related parameters from IVIM image data was successfully performed. We found that the perfusion-related parameters f and f·D* obtained with IVIM each had significant correlations with TBV and TBV obtained with DCE perfusion parameters.

The results of the present study revealed moderate or good correlations of tumor perfusion-related parameters between IVIM and DCE perfusion in patients with HNSCC. In their recent study, Federau et al. reported the correlation between perfusion-related parameters of both f and f·D* obtained with IVIM in brain tumors and that obtained with dynamic susceptibility contrast (DSC)-enhanced perfusion [13]; the correlation coefficient between f of IVIM and cerebral blood volume (CBV) of DSC

perfusion was 0.75, and the f·D* of IVIM and cerebral blood flow (CBF) of DSC perfusion was 0.65. In the present study, the correlation coefficients were rather lower for both f and f·D*. We suspect that the main reason for this discrepancy is that the susceptibility effect is greater in the head and neck than in intracranial lesions, and thus the signal intensity error caused by the susceptibility effect was apparent in the HNSCC. We think that this signal intensity error may have led to an insufficient signal-to-noise ratio (SNR) and incorrect fitting of multiple b-value data, and to finally result in the discrepancy between the values of f and D*. Notably, the correlation between f·D* obtained with IVIM and TBF with DCE perfusion was quite lower in the present study. We suspect that this was due to increased signal intensity error caused by the process of multiplication of the two parameters f and D*. It could be necessary to consider another model for IVIM parameters to convert TBF-related parameters without a process such as multiplication. However, Federau et al. also reported the correlation between f obtained with IVIM and CBV with the DSC method in brain glioma [25]. Kim et al. conducted a similar comparison of recurrent glioma and post-treatment tissue in the brain [26]. The Federau study reported the correlation coefficient of 0.59, which is slightly lower compared to our result. The correlation coefficient in the Kim et al. study was 0.67, which corresponds well with our result. The type of target lesion was quite

different between the present study and these two prior reports. Lesions with lower perfusion (such as low-grade gliomas) and post-treatment changes were included in the previous studies, whereas all of the subjects in our study had HNSCC, which are generally considered to have hyperperfusion. Notably, in the Federau study, the correlation in low-grade gliomas between f and CBV was very poor based on a scatterplot analysis. In our examination of HNSCCs, the signal decay in the range of low b-values which is well related to the signal decay from vascular component is thought to be larger due to its hypervascularity, and therefore the calculation of f can be more successfully performed compared to lesions with lower perfusion such as low grade glioma which is considered small signal change in low b-values. We suspect that factors such as the susceptibility effect and hyper- or hypo-perfusion in the target lesion have complex effects with both merits and demerits, finally resulting in a good or moderate correlation.

The results of the present study also suggest that there was a tendency for a difference to occur in calculated IVIM parameters between direct and asymptotic fitting. The correlation coefficients were greater in asymptotic fitting than direct fitting for both f and f･D*. We suspect that the reason for this is that the direct fitting of all three

parameters was greatly influenced by outliers in the signal intensity of several b-values, especially since the fitting of the bi-exponential function was used in the same manner as in the IVIM fitting. In addition, the signal intensity of EPI in HNSCCs sometimes includes large outliers caused by susceptibility or motion artifacts. However, both the mono-exponential fitting of the value D and the bi-exponential fitting of two parameters (f and D*) with constant D values are thought to involve less fitting error caused by outliers of signal intensity compared to the direct fitting of all three parameters, because the two parameters of f and D* will prevent the unstableness in f and D* in the least square fitting process more than all three parameters in direct fitting.

As another result of the present study, in direct fitting, the correlation coefficients between f and TBV, f·D* and TBF were respectively higher in the calculation by the ROI-based approach than that using f and f·D * maps of the pixel-by-pixel approach. This was probably because several pixels which contain an outlier of signal intensity will be averaged by using the mean value in the tumor ROI with the ROI-based approach, and conversely, outliers were directly used for the parameter calculation in the pixel-by-pixel approach, resulting in the greater fitting error and incorrect calculated value, especially using direct fitting. To improve such fitting errors, an ROI-based analysis can be useful with less fitting error for calculation, although the regional

distribution of IVIM parameters was not obtained in this method.

The present study has several limitations. First, the lower matrix of 64 × 64 in a 23-cm FOV was used to obtain the images with higher SNRs. Lesions with a large mass, such as the primary sites of many HNSCCs, were not considered problematic for the evaluation, but small lesions such as metastatic lymph nodes (< 1 cm dia.) can often be influenced by the partial volume effect, resulting in calculation errors because the signal intensity of the target lesion was not measured correctly by the partial volume effect. We should determine the ideal IVIM parameters with a higher matrix with an acceptable SNR and less image distortions for the reliable calculation of IVIM parameters, if we must evaluate such small lesions using IVIM.

Second, we used a total of 12 b-values for the calculation of IVIM parameters. Whether these b-points will be adequate for the parameter calculation was not investigated sufficiently in the present study. If the image quality and calculated parameters are fully reliable even if the b-values are decreased in IVIM acquisition, it would contribute to shortened scanning times.

A third limitation is that an analysis of reproducibility in the IVIM scanning was not conducted. This factor will be important for the assessment of the reliability of the

measurement of IVIM parameters. Further analyses are required to solve this question.

Fourth, the true diffusion coefficient ‘D’ was not compared to the gold standard of slow water diffusion. Slow water diffusion is well reflected by the tissue cellar density, because most of the water motion is restricted in the environment of large cellular spaces and small extracellular spaces [27]. This information cannot be obtained with DCE perfusion data only; histopathological information will be required. In addition, a comparison between D and the apparent diffusion coefficient (ADC) obtained from conventional DWI should be performed to determine which parameter best reflects the tissue cellular density.

Fifth, a different voxel size due to the difference of slice thickness and spatial resolution was used between the IVIM and DCE perfusion sequences. If a small ROI on a single slice is used for the measurement, an accurate comparison may not be obtained because of the large influence of the partial volume effect due to such different voxel sizes. However, the mean value of the whole-tumor ROI of all slices was used for the measurement in the present study. We therefore suspect that a large error induced by such a difference in voxel size was not involved in this comparison.

Sixth, the sample size was small, although a significant correlation was observed. Further studies are needed to address this limitation using larger study populations for

the measurement of more accurate correlation coefficients.

In conclusion, we found moderate or good correlations between IVIM-based results and DCE-based perfusion parameters in patients with HNSCC. In our calculation of IVIM parameters, asymptotic fitting was better correlated with DCE perfusion than direct fitting. The ROI-based analysis was also better correlated than the pixel-by-pixel basis analysis. The combination of asymptotic fitting and ROI-based analysis provided the best correlation, and a good correlation between f·D* and TBF was observed only in this combination. Careful selection of the calculation method in the measurement of perfusion-related parameters obtained with IVIM will be necessary for clinical applications.

REFERENCES

1. Srinivasan A, Mohan S, Mukherji SK. Biologic imaging of head and neck cancer: the present and the future. AJNR Am J Neuroradiol 2012;33:586-594.

2. Takayama Y, Ohno T, Kishimoto R, Kato S, Yoneyama R, Kandatsu S, Tsujii H, Obata T. Prediction of early response to radiotherapy of uterine carcinoma with dynamic contrast-enhanced MR imaging using pixel analysis of MR perfusion imaging. Magn Reson Imaging 2009;27:370-376.

3. Pauls S, Mottaghy FM, Schmidt SA, Kruger S, Moller P, Brambs HJ, Wunderlich, A. Evaluation of lung tumor perfusion by dynamic contrast-enhanced MRI. Magn Reson Imaging 2008;26:1334-1341.

4. Agrawal S, Awasthi R, Singh A, Haris M, Gupta RK, Rathore RK. An exploratory study into the role of dynamic contrast-enhanced (DCE) MRI metrics as predictors of response in head and neck cancers. Clin Radiol 2012;67:e1-5.

5. Sumi M, Nakamura T. Head and neck tumours: combined MRI assessment based on IVIM and TIC analyses for the differentiation of tumors of different histological types. Eur Radiol 2014;24:223-231.

6. Chawla S, Kim S, Dougherty L, Wang S, Loevner LA, Quon H, Poptani H. .Pretreatment diffusion-weighted and dynamic contrast-enhanced MRI for prediction of local treatment response in squamous cell carcinomas of the head and neck. AJR Am J Roentgenol 2013;200:35-43.

7. Shukla-Dave, Lee NY, Jansen JF, Thaler HT, Stambuk HE, Fury MG, Patel SG, Moreira AL, Sherman E, Karimi S, Wang Y, Kraus D, Shah JP, Pfister DG, Koutcher JA. Dynamic contrast-enhanced magnetic resonance imaging as a predictor of outcome in head-and-neck squamous cell carcinoma patients with nodal metastases. Int J Radiat Oncol Biol Phys 2012;82:1837-1844.

8. Le Bihan D, Breton E, Lallemand D, Aubin ML, Vignaud J, Laval-Jeantet M. Separation of diffusion and perfusion in intravoxel incoherent motion MR imaging. Radiology 1988;168:497-505.

9. Marzi S, Piludu F, Vidiri A. Assessment of diffusion parameters by intravoxel incoherent motion MRI in head and neck squamous cell carcinoma. NMR Biomed 2013;26:1806-1814.

10. Le Bihan D, Turner R, MacFall JR. Effects of intravoxel incoherent motions (IVIM) in steady-state free precession (SSFP) imaging: application to molecular diffusion imaging. Magn Reson Med 1989;10:324-337.

11. Kakite S, Dyvorne H, Besa C, Cooper N, Facciuto M, Donnerhack C, Taouli, B. Hepatocellular carcinoma: Short-term reproducibility of apparent diffusion coefficient and intravoxel incoherent motion parameters at 3.0T. J Magn Reson Imaging 2014; in press.

12. Wirestam R, Borg M, Brockstedt S, Lindgren A, Holtas S, Stahlberg F. Perfusion-related parameters in intravoxel incoherent motion MR imaging compared with CBV and CBF measured by dynamic susceptibility-contrast MR technique. Acta Radiol 2001;42:123-128.

13. Federau C, O'Brien K, Meuli R, Hagmann P, Maeder P. Measuring brain perfusion with intravoxel incoherent motion (IVIM): Initial clinical experience. J Magn Reson Imaging 2014; in press.

14. Dopfert J, Lemke A, Weidner A, Schad LR. Investigation of prostate cancer using diffusion-weighted intravoxel incoherent motion imaging. Magn Reson Imaging 2011;29:1053-1058.

15. Hauser T, Essig M, Jensen A, Gerigk L, Laun FB, Munter M, Simon D, Stieltjes B. Characterization and therapy monitoring of head and neck carcinomas using diffusion-imaging-based intravoxel incoherent motion parameters-preliminary results. Neuroradiology 2013;55:527-536.

16. Anzai Y, Lufkin RB, Jabour BA, Hanafee WN. Fat-suppression failure artifacts simulating pathology on frequency-selective fat-suppression MR images of the head and neck. AJNR Am J Neuroradiol 1992;13:879-884.

17. Sourbron SP, Buckley DL. Tracer kinetic modelling in MRI: estimating perfusion and capillary permeability. Phys Med Biol 2012;57:R1-33.

18. Brix G, Semmler W, Port R, Schad LR, Layer G, Lorenz WJ. Pharmacokinetic parameters in CNS Gd-DTPA enhanced MR imaging. J Comput Assist Tomogr 1991;15:621-628.

19. Wu WC, Su MY, Chang CC, Tseng WY, Liu KL. Renal perfusion 3-T MR imaging: a comparative study of arterial spin labeling and dynamic contrast-enhanced techniques. Radiology 2011;261:845-853.

20. Thomassin-Naggara I, Balvay D, Aubert E, Darai E, Rouzier R, Cuenod CA, Bazot M. Quantitative dynamic contrast-enhanced MR imaging analysis of complex adnexal masses: a preliminary study. Eur Radiol 2012;22:738-745.

21. Ichikawa S, Motosugi U, Ichikawa T, Sano K, Morisaka H, Araki T. Intravoxel incoherent motion imaging of the kidney: alterations in diffusion and perfusion in patients with renal dysfunction. Magn Reson Imaging 2013;31:414-417.

22. Lee JT, Liau J, Murphy P, Schroeder ME, Sirlin CB, Bydder M. Cross-sectional

investigation of correlation between hepatic steatosis and IVIM perfusion on MR imaging. Magn Reson Imaging 2012;30:572-578.

23. Sumi M, Nakamura T. Head and neck tumors: assessment of perfusion-related parameters and diffusion coefficients based on the intravoxel incoherent motion model. AJNR Am J Neuroradiol 2013;34:410-416.

24. Lee HJ, Rha SY, Chung YE, Shim HS, Kim YJ, Hur J, Hong YJ, Choi BW. Tumor perfusion-related parameter of diffusion-weighted magnetic resonance imaging: Correlation with histological microvessel density. Magn Reson Med 2014;71:1554-1558.

25. Federau C, Meuli R, O'Brien K, Maeder P, Hagmann P. Perfusion measurement in brain gliomas with intravoxel incoherent motion MRI. AJNR Am J Neuroradiol 2014;35:256-262.

26. Kim HS, Suh CH, Kim N, Choi CG, Kim SJ. Histogram analysis of intravoxel incoherent motion for differentiating recurrent tumor from treatment effect in patients with glioblastoma: initial clinical experience. AJNR Am J Neuroradiol 2014;35:490-497.

27. Gupta RK, Cloughesy TF, Sinha U, Garakian J, Lazareff J, Rubino G, Rubino L, Becker DP, Vinters HV, Alger JR. Relationships between choline magnetic

resonance spectroscopy, apparent diffusion coefficient and quantitative histopathology in human glioma. J Neurooncol 2000;50:215-226.

Figure Legends

Fig. 1. The two-compartment model used for the DCE perfusion analysis. The model assumed that the plasma and extravascular extracellular space (EES) are both compartments. In this model, the indicator (=contrast agent) flows from an arterial inlet into the plasma, and also flows out of the plasma to the venous outflow. In addition, the indicator particles extracted through the capillary wall will pass through the EES from the plasma, and will also leak back into the plasma at the same time with the exchange rate of the permeability surface product.

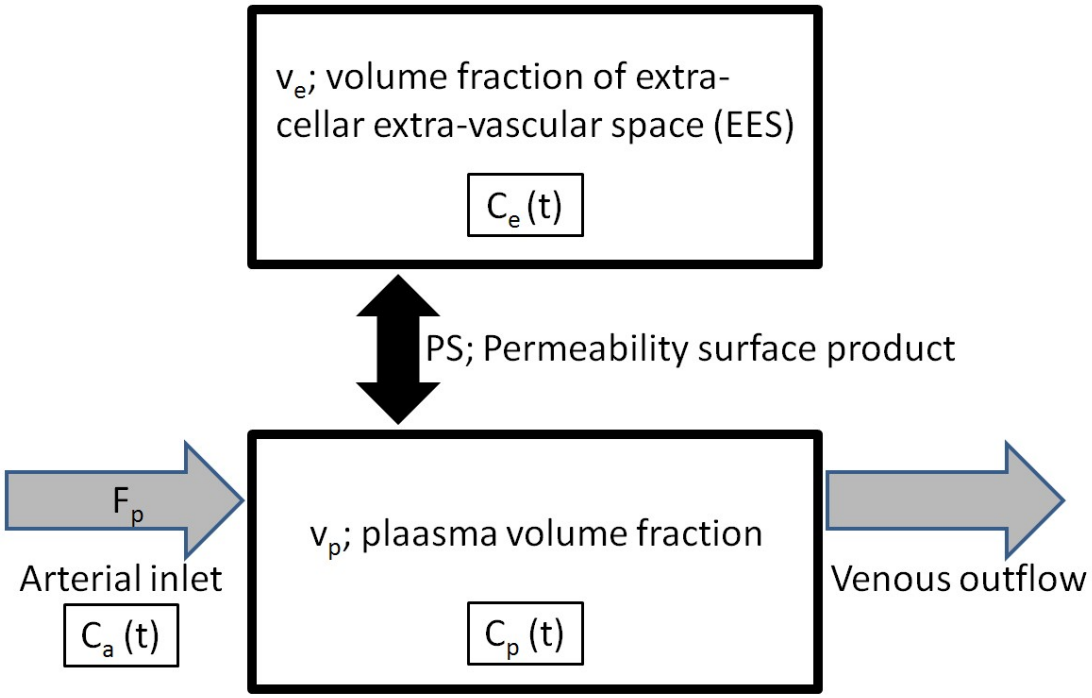


Fig. 2. Tumor delineation to determine the tumor region of interest (ROI) in IVIM imaging with the pixel-by-pixel approach. Each tumor was delineated with a polygonal ROI on IVIM raw images (b=0) for the IVIM analysis (a) with the reference of post-contrast-enhanced 3D-T1 images (b; arrow). The delineated ROI for IVIM analysis was copied on f and f·D* map which were obtained with pixel-by-pixel basis from the each pixel's signal intensity in the IVIM data with direct fitting (c, d) and with asymptotic fitting (e, f).

Fig.2a 

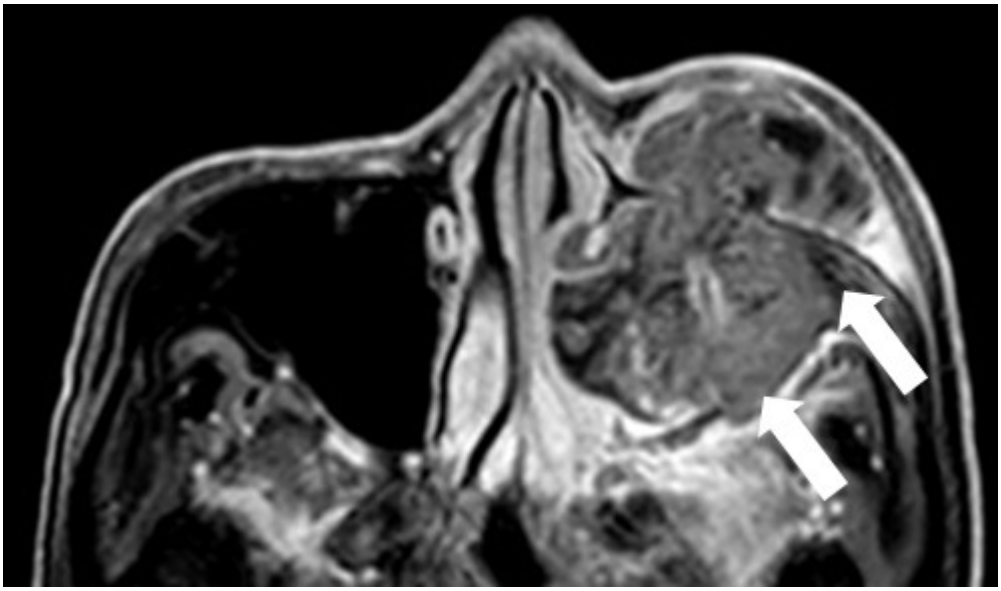


Fig.2b

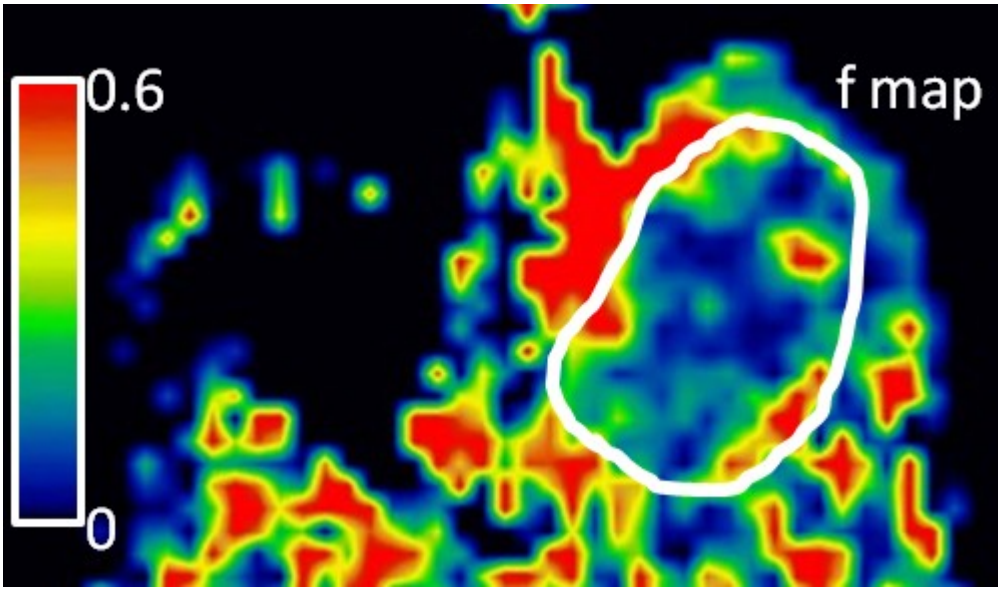


Fig.2c

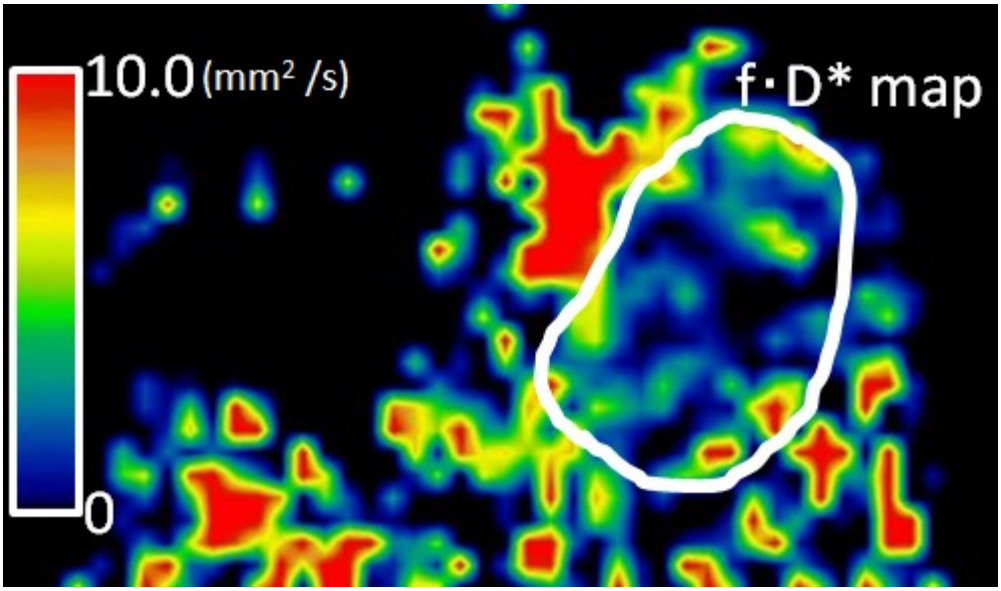


Fig.2d

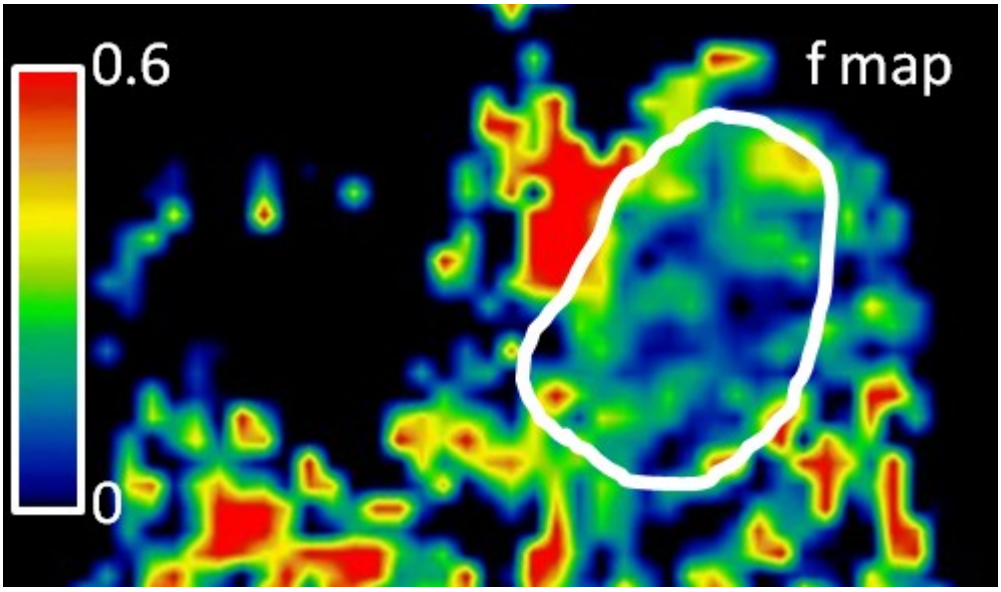


Fig.2e

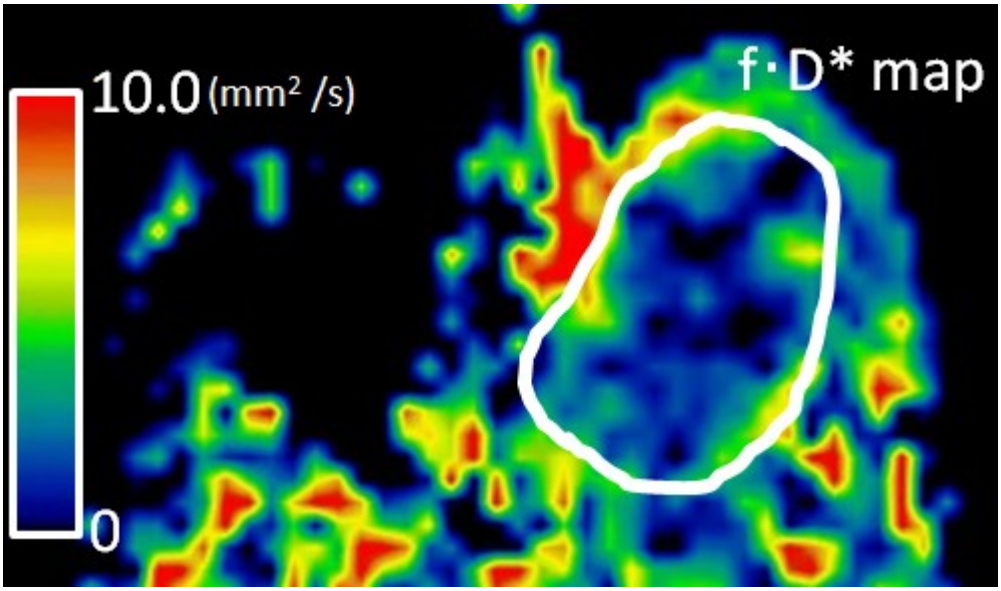
Fig.2f 

Fig. 3. Tumor delineation to determine the tumor region of interest (ROI) in IVIM using the ROI-based approach. Each tumor was delineated with a polygonal ROI on IVIM raw images (b=0) (a; arrow) with the reference of post-contrast-enhanced 3D-T1 images (b; arrow), and then the ROI was copied in EPI images of each b-value (a; arrowhead). The mean values of these ROIs were respectively calculated and defined as the image signal intensity for each b-value. Finally, by using these mean values in the ROI of each b-value, we calculated the IVIM parameters of f and f・D* in both direct and asymptotic fitting.

Fig.3a

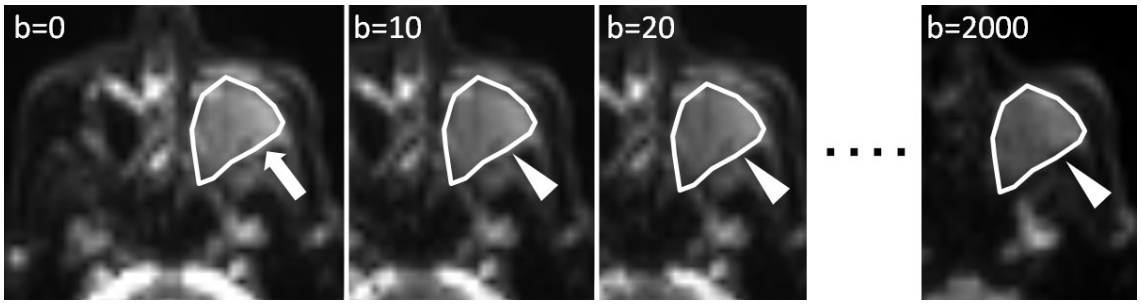


Fig.3b

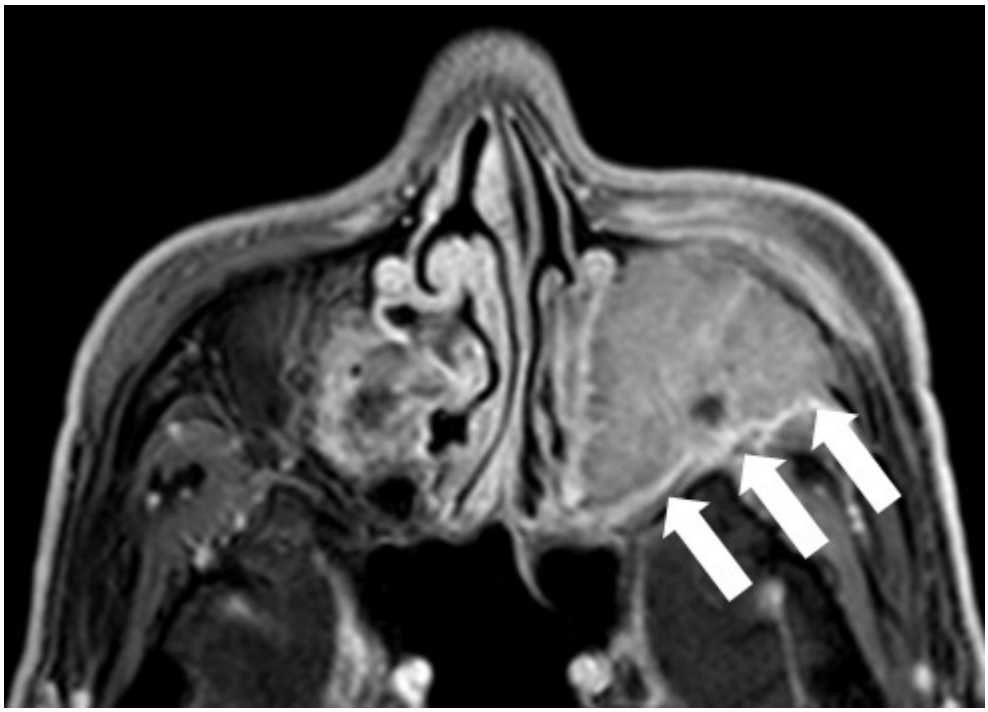


Fig. 4. Scatterplot of f-values obtained with IVIM and TBV with DCE perfusion. In the pixel-by-pixel approach, a moderate correlation was observed between f and TBV with direct fitting ($r = 0.53$, $y = 0.011x - 0.046$) (a), whereas a good correlation was observed with asymptotic fitting ($r = 0.65$, $y = 0.007x - 0.070$) (b). A good correlation

in both direct and asymptotic fitting was observed in the ROI-based approach (direct fitting; r = 0.62, y = 0.007x − 0.073, asymptotic fitting; r = 0.68, y = 0.006x − 0.068) (c, d).

Fig.4a

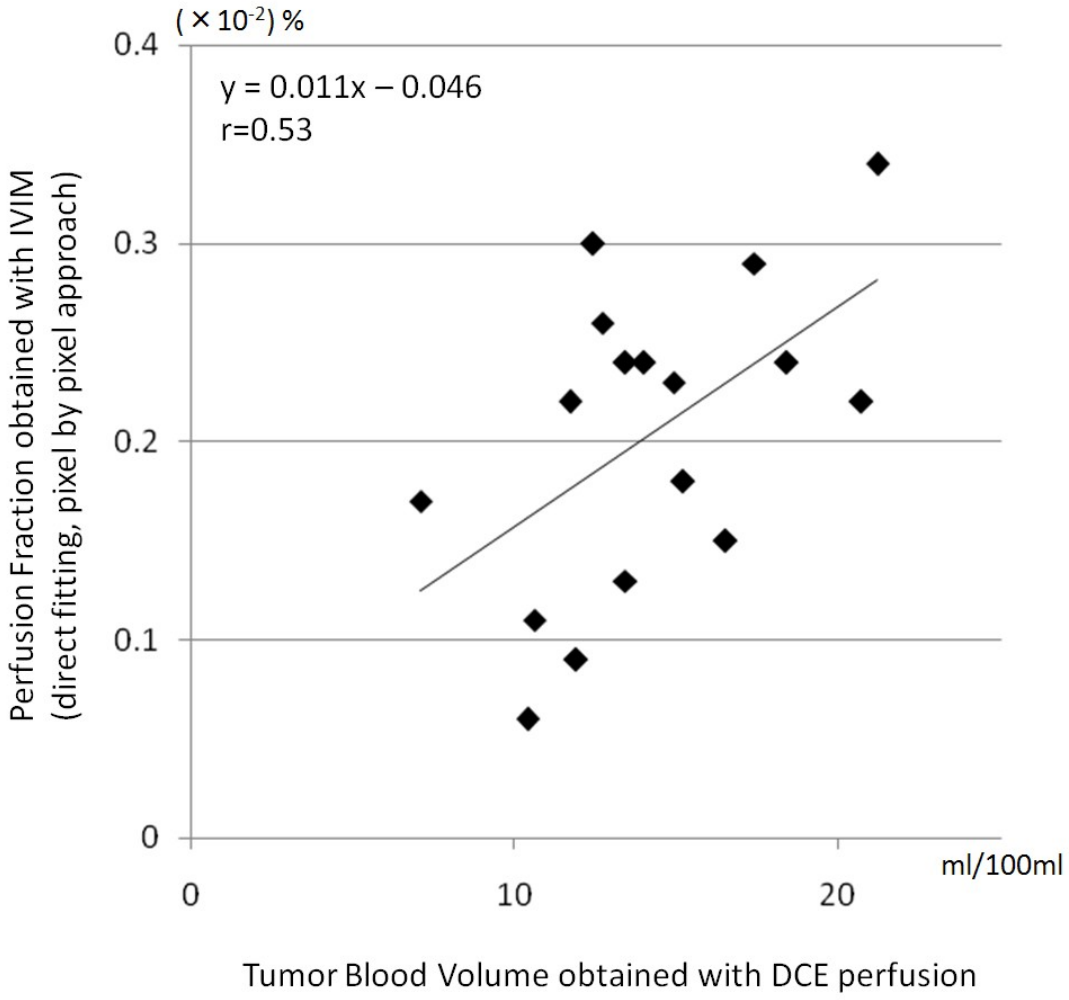


Fig.4b

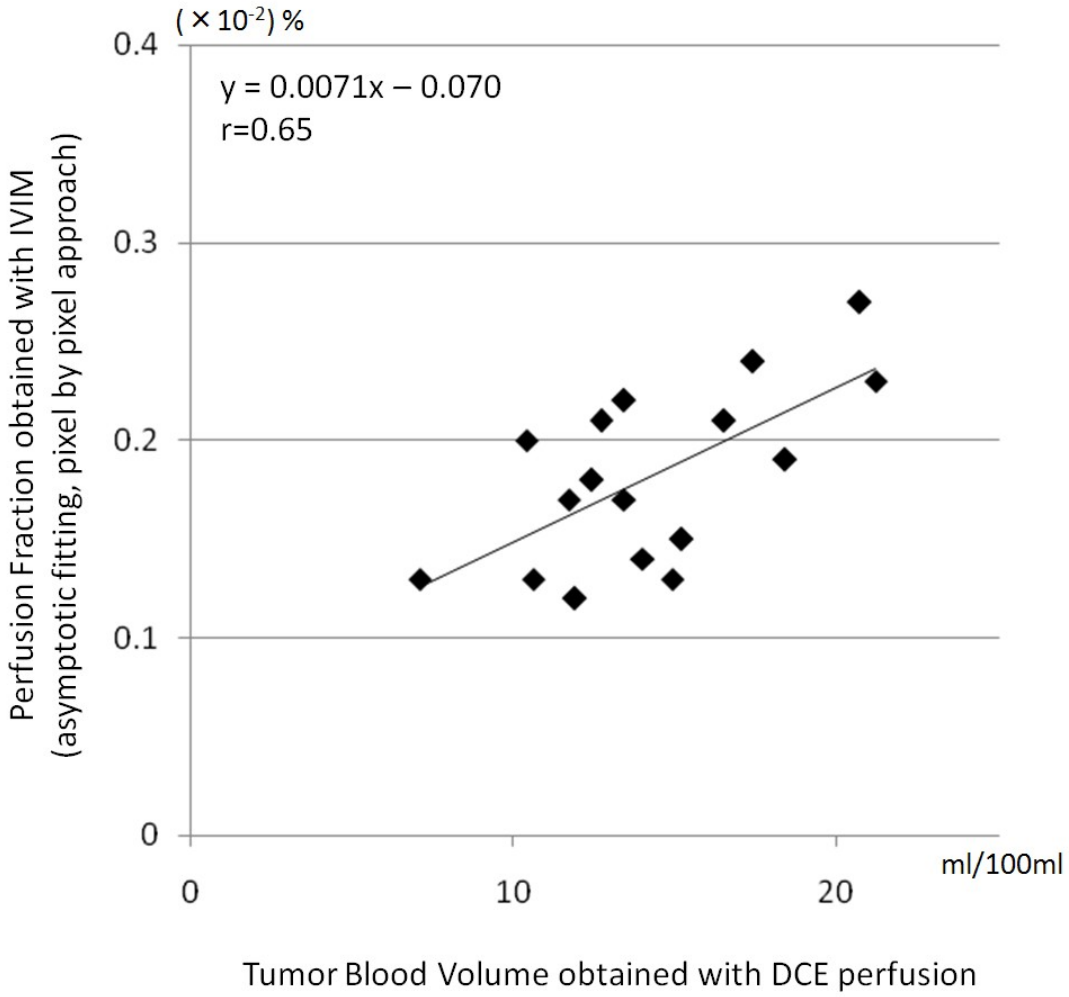

(×10-2) %
0.4
0.3
0.2
0.1
0
y = 0.0071x – 0.070
r=0.65
Perfusion Fraction obtained with IVIM
(asymptotic fitting, pixel by pixel approach)
0
10
20
ml/100ml
Tumor Blood Volume obtained with DCE perfusion

Fig.4c

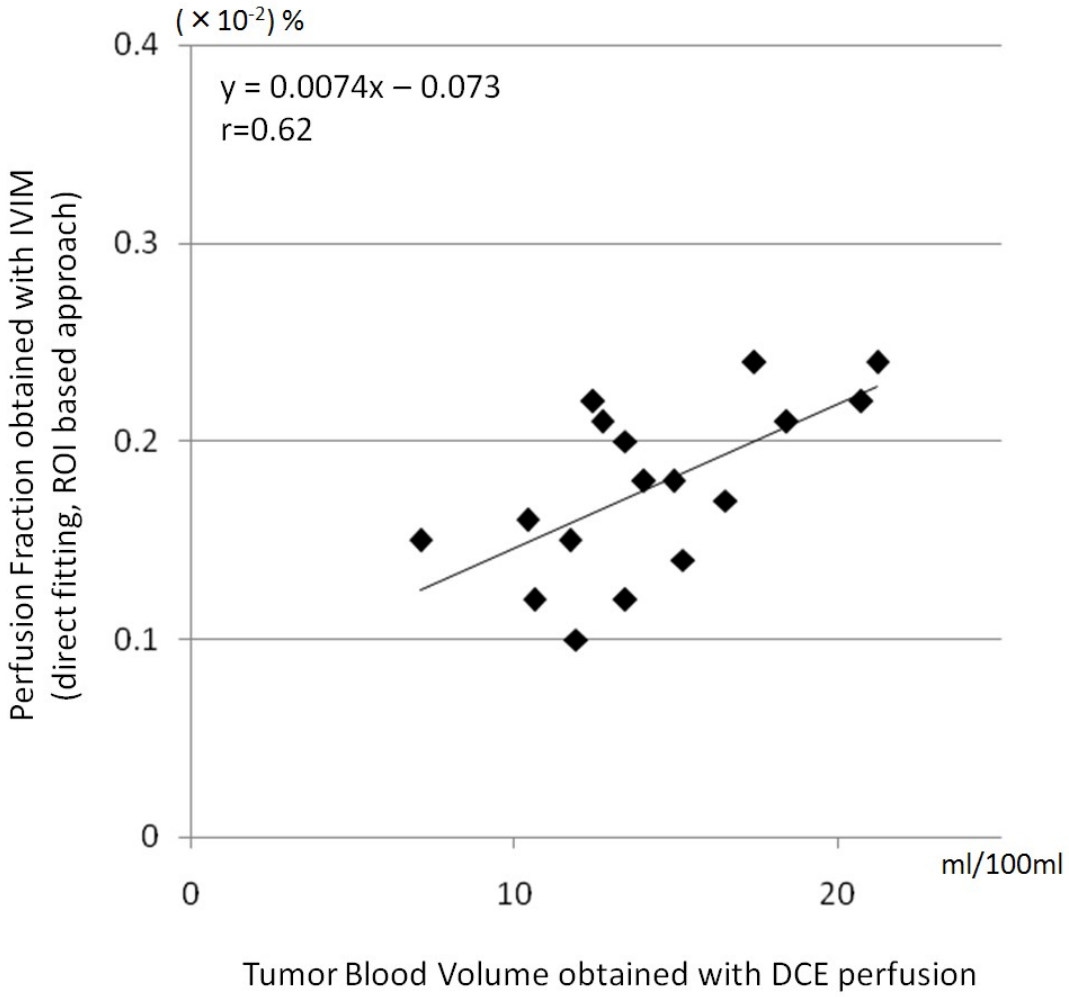

(×10-2) %
0.4
0.3
0.2
0.1
0
y = 0.0074x – 0.073
r=0.62
Perfusion Fraction obtained with IVIM
(direct fitting, ROI based approach)
0
10
20
ml/100ml
Tumor Blood Volume obtained with DCE perfusion

Fig.4d

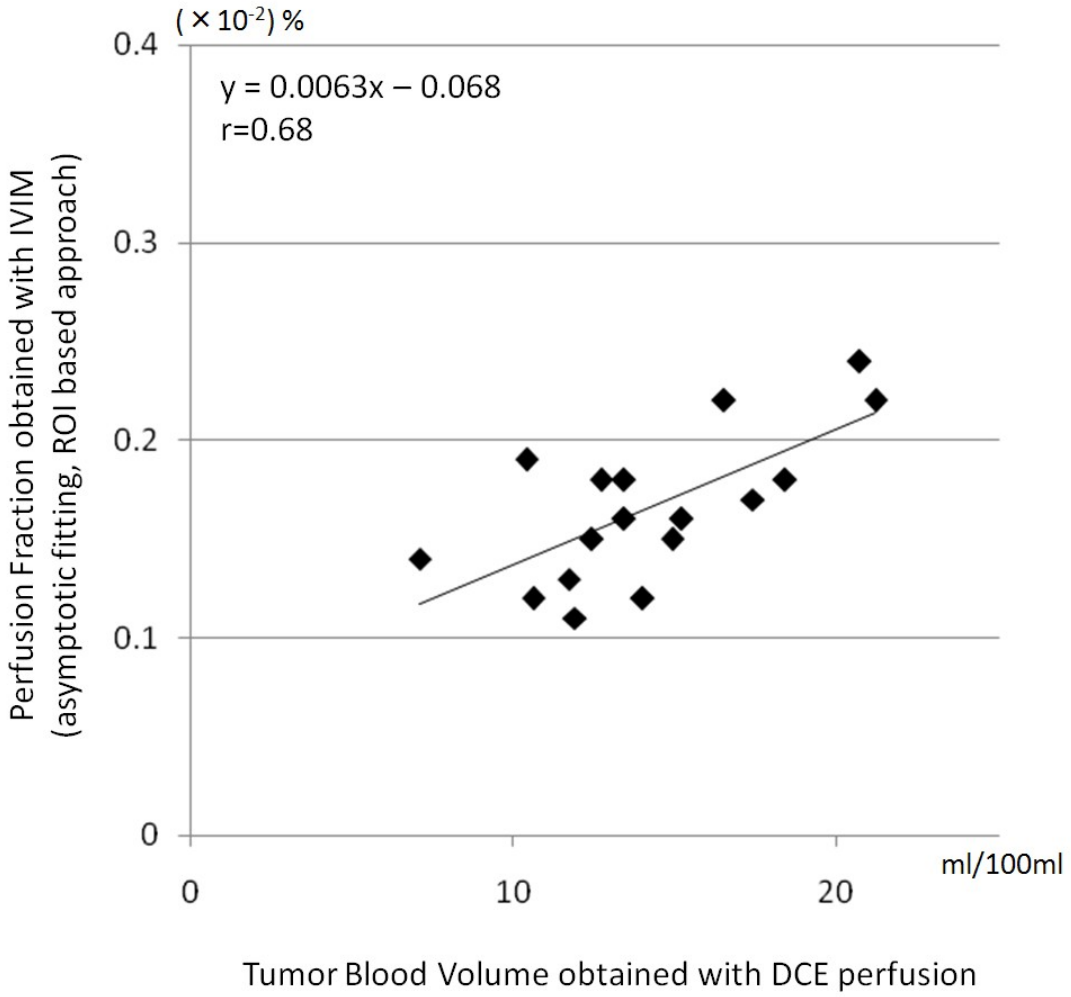


Fig. 5. Case example of both direct and asymptotic fitting. The decay of signal intensity in each b-value and IVIM fitting curve using the three calculated parameters (D, D*, f) obtained from both the direct and asymptotic methods in a representative pixel is shown. We suspected that there was an outlier in the b-value of 2000 (arrow) because the decrease of signal intensity was very small compared to that in the b-value of 1000. The

calculated value by direct fitting was probably influenced by this outlier, resulting in a not well-fitted b-value for 0–400 (arrowhead).

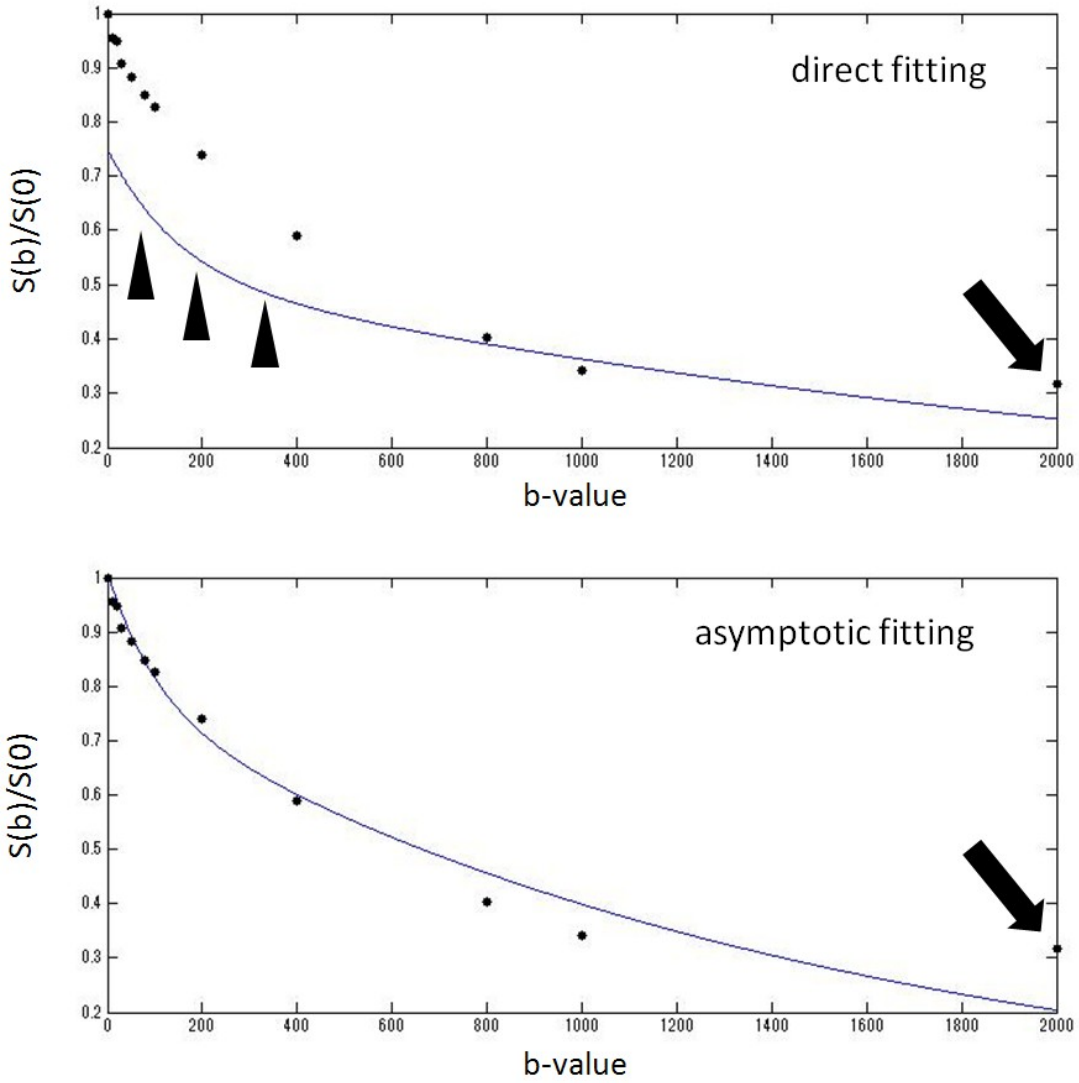


Fig. 6. Scatterplot of f・D* values obtained with IVIM and TBV with DCE perfusion. In the pixel-by-pixel approach, a moderate correlation was observed in both direct fitting (r = 0.47, y = 0.030x − 1.2) (a) and asymptotic fitting (r = 0.54, y = 0.026x − 1.3) (b). A

moderate correlation was also observed in direct fitting with the ROI-based approach (r = 0.52, y = 0.019x − 0.27) (c). In contrast, a good correlation was observed in asymptotic fitting with the ROI-based approach (r = 0.65, y = 0.021x − 0.92) (d).

Fig.6a

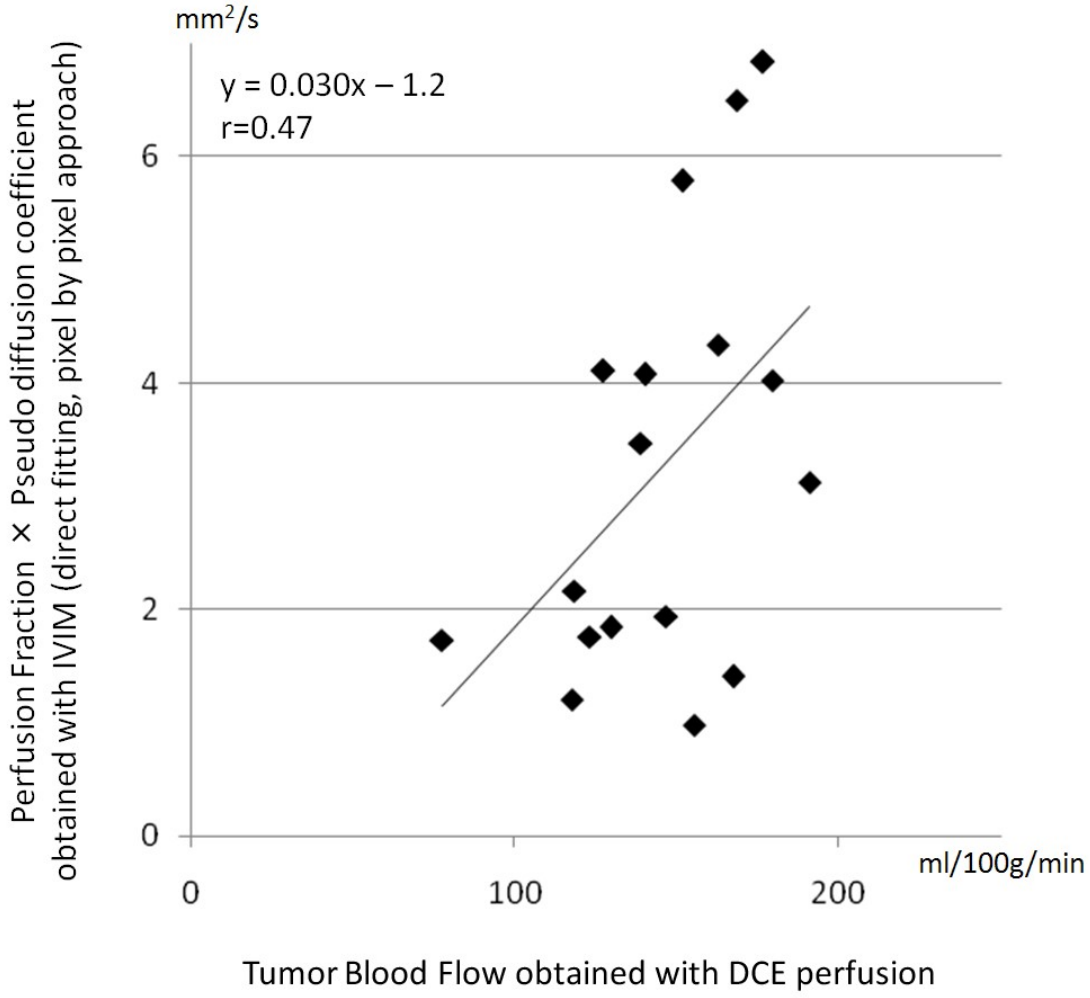


Fig.6b

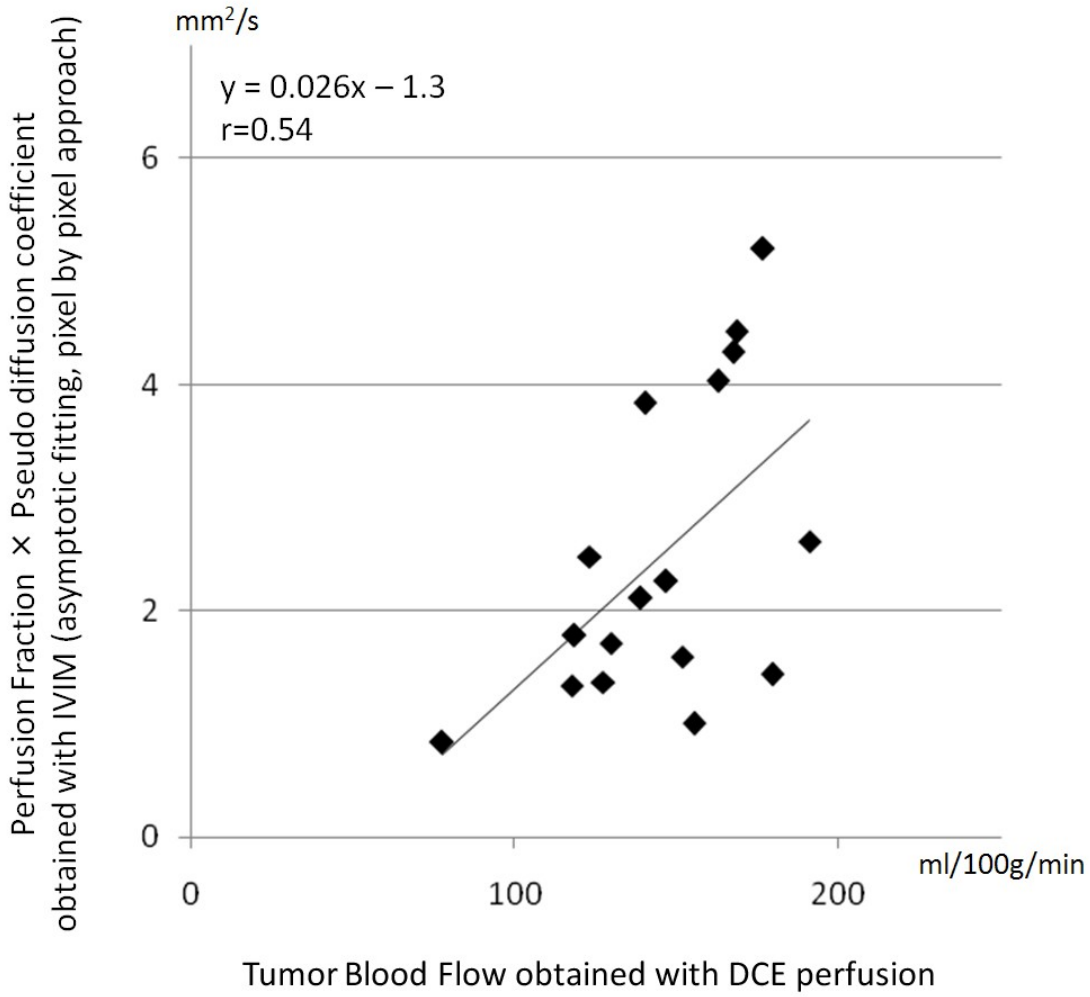

mm²/s
y = 0.026x – 1.3
r=0.54
6
4
2
0
0
100
200
ml/100g/min
Perfusion Fraction × Pseudo diffusion coefficient
obtained with IVIM (asymptotic fitting, pixel by pixel approach)
Tumor Blood Flow obtained with DCE perfusion

Fig.6c

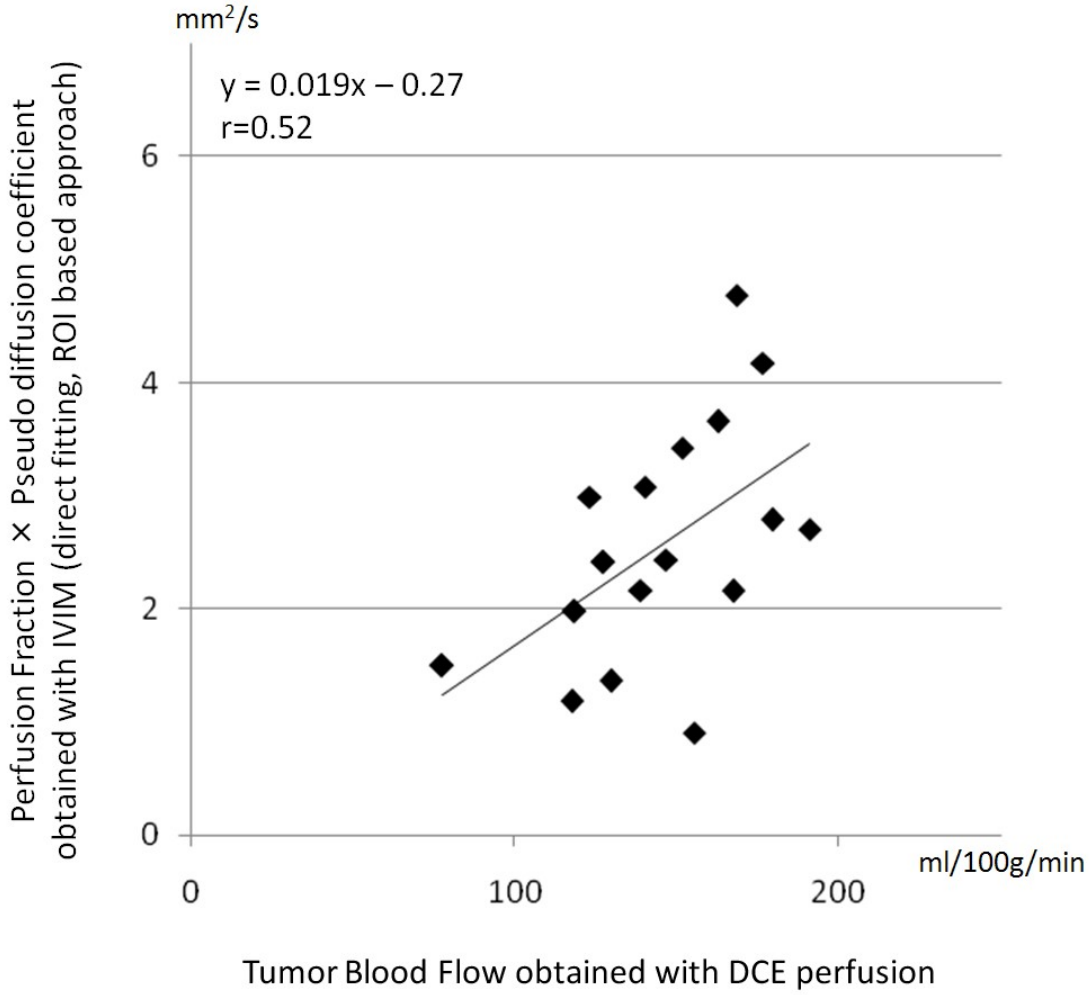
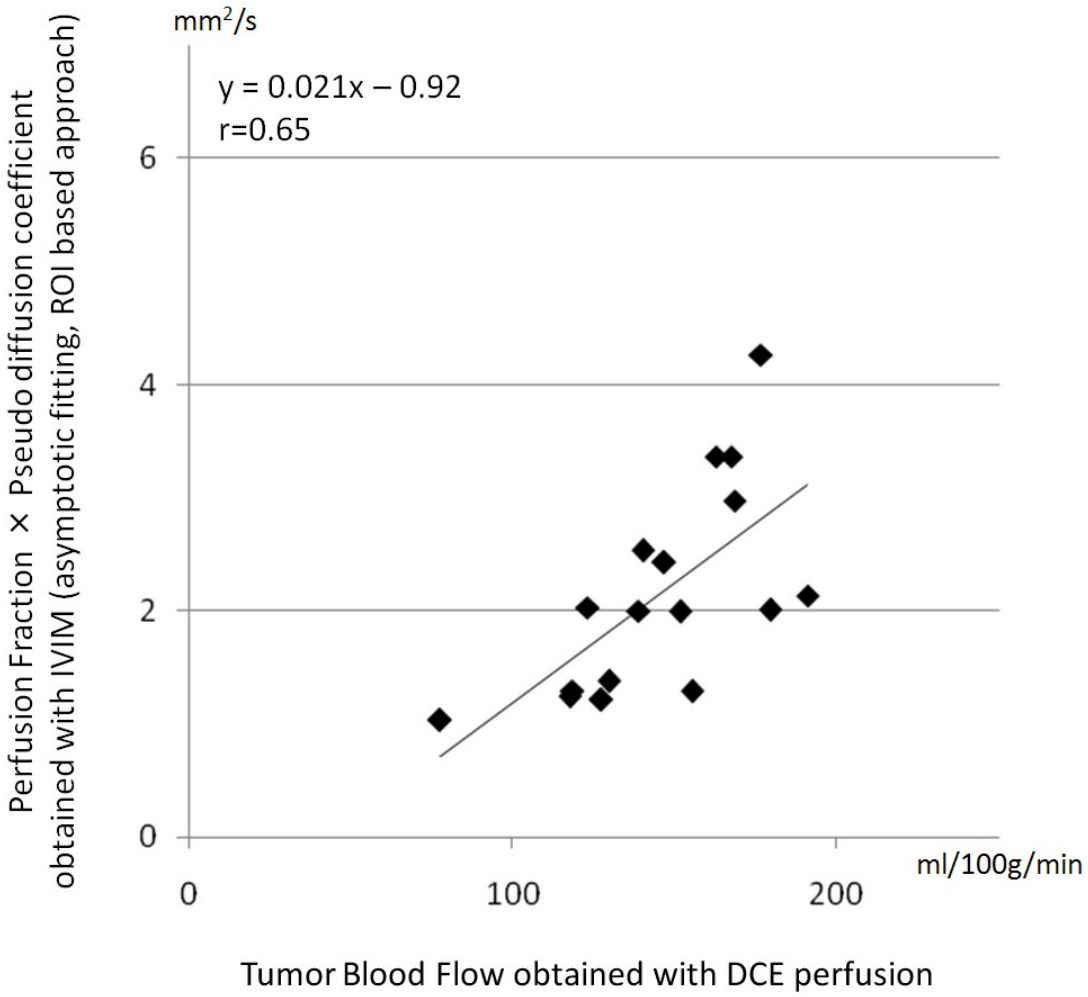

mm²/s
y = 0.019x – 0.27
r=0.52
6
4
2
0
0
100
200
ml/100g/min
Perfusion Fraction × Pseudo diffusion coefficient obtained with IVIM (direct fitting, ROI based approach)
Tumor Blood Flow obtained with DCE perfusion

Fig.6d


mm²/s
y = 0.021x – 0.92
r=0.65
6
4
2
0
0
100
200
ml/100g/min
Perfusion Fraction × Pseudo diffusion coefficient
obtained with IVIM (asymptotic fitting, ROI based approach)
Tumor Blood Flow obtained with DCE perfusion